



Article

The Complete Genome Sequence, Molecular Detection, and Anatomical Analysis of Hibiscus Chlorotic Ringspot Virus Infecting *Hibiscus rosa-sinensis* in Peninsular Malaysia

Mohd Shakir Mohamad Yusop ¹, Normawati Lanisa ², Noraini Talip ², Mohd Faiz Mat Saad ¹, Azlan Abas ³, Murni Nazira Sarian ¹, Hamizah Shahirah Hamezah ¹, Sarahani Harun ¹ and Hamidun Bunawan ^{1,*}

¹ Institute of Systems Biology (INBIOSIS), Universiti Kebangsaan Malaysia, UKM, Bangi 43600, Selangor, Malaysia; shakir.yusop@gmail.com (M.S.M.Y.); faizsaad@ukm.edu.my (M.F.M.S.);

murninazira@ukm.edu.my (M.N.S.); hamizahshahirah@ukm.edu.my (H.S.H.); sarahani@ukm.edu.my (S.H.)
² Department of Biotechnology and Biological Sciences, Faculty of Science and Technology, Universiti Kebangsaan Malaysia, UKM, Bangi 43600, Selangor, Malaysia; normawatil.2608@gmail.com (N.L.); ntalip@ukm.edu.my (N.T.)

³ Center for Research in Development, Social and Environment (SEEDS), Faculty of Social Sciences and Humanities, Universiti Kebangsaan Malaysia, UKM, Bangi 43600, Selangor, Malaysia; azlanabas@ukm.edu.my

* Correspondence: hamidun.bunawan@ukm.edu.my

Abstract: *Hibiscus rosa-sinensis* is the national flower of Malaysia and is widely cultivated as landscape planting across the nation. In 1995, Hibiscus chlorotic ringspot virus (HCRSV) was reported for the first time in Malaysia. Until today, there have been no follow-up studies on the viral infection in the plant, yet the virus symptom of chlorotic spots has been observed throughout the *Hibiscus* population. Therefore, this study aimed to report the complete genome sequence of the HCRSV, validate a molecular detection tool for its diagnosis, and measure the impact of the virus symptom and infection in *H. rosa-sinensis*. This study reported the complete genome of the HCRSV through RNA sequencing. The phylogenetic analysis of the HCRSV isolated from different geographical sources and several other related viruses was performed to confirm its identity and classification. Additionally, primers based on the genome sequence were designed and used for RT-PCR to detect the presence of the virus in symptomatic leaves, further confirming the HCRSV identity and presence. Meanwhile, the impact of the virus was measured by examining the anatomical and morphological changes in the leaf structure of symptomatic samples. Light microscopy and scanning electron microscopy were used to examine potential adaptations and comparisons between the leaf structures of healthy and infected samples, especially in the leaf lamina, petiole, and midrib cells. The results confirmed the complete genome sequence of the HCRSV, its molecular detection strategy, and the impact of the viral infection on *Hibiscus* leaves in Peninsular Malaysia. This study is beneficial for the management strategy of the virus and for protecting an important plant in the nation.

Keywords: anatomy; complete genome; Hibiscus chlorotic ringspot virus; *Hibiscus rosa-sinensis*; micromorphology; RT-PCR



Citation: Yusop, M.S.M.; Lanisa, N.; Talip, N.; Mat Saad, M.F.; Abas, A.; Sarian, M.N.; Hamezah, H.S.; Harun, S.; Bunawan, H. The Complete Genome Sequence, Molecular Detection, and Anatomical Analysis of Hibiscus Chlorotic Ringspot Virus Infecting *Hibiscus rosa-sinensis* in Peninsular Malaysia. *Horticulturae* **2023**, *9*, 569. <https://doi.org/10.3390/horticulturae9050569>

Academic Editors: Vladimir K. Chebotar and Anastasiya M. Kamionskaya

Received: 16 March 2023

Revised: 17 April 2023

Accepted: 30 April 2023

Published: 11 May 2023



Copyright: © 2023 by the authors. Licensee MDPI, Basel, Switzerland. This article is an open access article distributed under the terms and conditions of the Creative Commons Attribution (CC BY) license (<https://creativecommons.org/licenses/by/4.0/>).

1. Introduction

Hibiscus rosa-sinensis L. is a malvaceous perennial shrub that has been cultivated as ornamentals in different countries across multiple regions, such as Malaysia, Singapore, India, China, Hawaii, Brazil, Iran, and Nigeria [1–7]. *H. rosa-sinensis* is susceptible to plant viruses including Hibiscus chlorotic ringspot virus (HCRSV), Hibiscus latent Singapore virus (HLSV), Hibiscus latent ringspot virus (HLRSV), Hibiscus latent Fort Pierce virus (HLFPV), and Hibiscus green spot virus (HGSV) [8–12]. In addition, viruses could develop symptoms that reduce the ornate value of *H. rosa-sinensis* [13,14]. One of the most prevalent viruses found throughout the global population of *H. rosa-sinensis* is the HCRSV [15,16].

HCRSV is a positive-sense, single-stranded RNA virus that belongs to the family *Tombusviridae* (genus: *Betacarmovirus*) with an isometric monopartite virus structure of 28 nm in diameter [15,17]. The occurrence of the HCRSV in *H. rosa-sinensis* was first identified in the cultivars exported from El Salvador into the United States of America [12]. Since then, the virus has been identified in *H. rosa-sinensis* cultivated throughout the globe [6,7,15,16,18–23]. A distinct characteristic of the HCRSV is that the virus can encode a total of seven open reading frames (ORFs): the typical five of a *Carmovirus*, in addition to two novel ORFs, namely, ORF (p23) and ORF (p25) [15,24]. Figure 1 shows the schematic representation of the genome and encoded proteins. The HCRSV genomic RNA (gRNA) contains around 3900 nucleotides (nt) with a t-RNA-like structure at the 3′ terminal. Closest to the 5′ terminal, the ORF (p28) encodes a product with an apparent molecular mass of 28 kDa. ORF (p81) is the product of the readthrough of ORF (p28). ORF (p8) and ORF (p9) are in the centre of the genome and overlap each other. Near the 3′ terminal, ORF (p38) is present. The two novel ORFs, ORF (p23) and ORF (p25) are within ORF (p28) and ORF (p38), respectively [15,24].

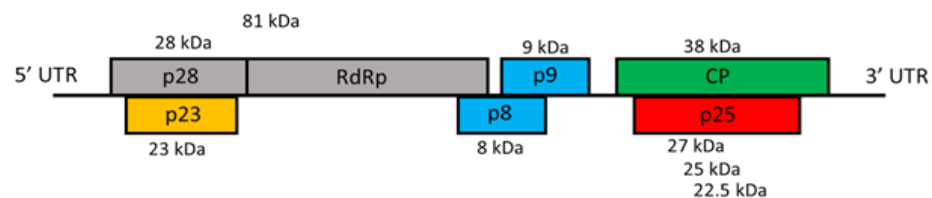


Figure 1. Schematic representation of the HCRSV genome organisation showing the proteins encoded from the seven ORFs. The kDa values indicate the sizes of the putative proteins and isoforms. Figure adapted from [17].

The products encoded from ORF (p28) and the readthrough ORF (p81) are putatively the subunits of viral replicase, while the p8 and p9 proteins—encoded from ORF (p8) and ORF (p9), respectively—are required for virus movement [15]. The p23 protein encoded from ORF (p23) is essential for host-specific replication [25]. Interestingly, ORF (p25) has the potential to encode three protein isoforms—namely, p27, p25, and p22.5 proteins—where all of these play a role in symptom expression and virus movement throughout the host [24]. ORF (p38) was found to encode viral coat protein (CP), which is important for encapsidation and systemic movement of the virus [15,26]. The CP of the HCRSV is vital for long-distance cell-to-cell movement and post-transcriptional gene silencing in host plants [27,28].

The common symptoms of host plants infected with the HCRSV include leaf mottling, chlorotic spots, vein banding patterns, and stunted growth [12,15]. The HCRSV was found to infect Malaysian *H. rosa-sinensis* more than two decades ago [18]. To our knowledge, no further research has been done on the HCRSV in Malaysia, including on the virus's complete nucleotide sequence of the Malaysian isolate.

This study examined the infection of the HCRSV and its impact on the host, namely, *H. rosa-sinensis*. Hence, three things are reported here: (1) the complete nucleotide sequence and genome structure of the Malaysian isolate of the HCRSV, (2) the detection strategy used to identify the viral presence, and (3) the anatomical and morphological changes in the leaves of *H. rosa-sinensis* exhibiting the chlorotic spots symptom caused by the HCRSV.

2. Materials and Methods

2.1. Plant Material

Surveys on the *H. rosa-sinensis* landscape plants were done to examine the presence of the chlorotic spots symptom associated with a viral infection. Symptomatic leaves were collected from different individual plants with similar positions based on height and size (the leaves from one individual plant were considered as one sample) [29]. A total number of 31 symptomatic samples were collected from different *H. rosa-sinensis* populations across five regions in Malaysia: the states of Selangor, Negeri Sembilan, Perak, Pahang, and the Federal Territory of Putrajaya. The samples were taken fresh and maintained in an icebox

for transportation before being kept at -80°C . Table 1 records the quantity of the collected samples and their locations.

Table 1. List of the quantities of collected leaf samples of *H. rosa-sinensis* with the symptoms and respective locations.

Symptom	Location (Google Coordinates)	Quantity of Samples
Foliar chlorotic spots	Bangi, Selangor (2.96641, 101.78868)	5
	UKM, Selangor (2.92528, 101.773)	5
	Nilai, Negeri Sembilan (2.80842, 101.81312)	7
	Ipoh, Perak (4.62352, 101.06852)	4
	Raub, Pahang (3.79353, 101.85746)	5
	Putrajaya (2.92424, 101.6892)	5
		Total: 31

2.2. RNA Extraction

The total RNA was extracted from the symptomatic samples using the QIAGEN RNeasy Plant Mini Kit (QIAGEN, Hilden, Germany) according to the manufacturer's protocol. The samples were then analysed on a Nanodrop instrument and kept at -80°C before further use.

2.3. RNA Sequencing

The RNA extract was pooled and sent for sequencing using Illumina HiSeq 2500 platform (1st BASE Sequencing Malaysia, Selangor, Malaysia). The RNA samples were subjected to library preparation at the 1st BASE Sequencing Facility using the TruSeq-stranded Total RNA sample preparation Ribo-Zero plant kit (Illumina) with quality control. Then, the samples were run on the HiSeq 2500 platform with a TruSeq SBS version 4 kit (Illumina, Universiti Kebangsaan Malaysia, Selangor, Malaysia) with 150 cycles of paired-end reads. The data were then used for de novo assembly through Trinity 2.8.4 with default settings [30]. Finally, megaBLAST analysis against the NCBI database was performed on the assembled transcripts to identify any contigs with high sequence similarity.

2.4. Computational and Phylogenetic Analysis

The contig was then further analysed through online resources, including NCBI-ORF Finder and Expasy. The contig was also used with other genome sequences as the input for a similarity plot made with SimPlot software. SimPlot is generally used to plot the percentage identity of the input sequences to a reference sequence [31].

Identity and similarity percentages, multiple sequence alignment, and phylogenetic determination were performed using MEGA software with its built-in functions [32,33]. Complete sequences for the relevant viruses within their genus were acquired through the BLASTn function in MEGA X. The complete genome sequences within the *Betacarmovirus* were selected and subjected to multiple sequence alignments using the MUSCLE program function. Finally, the phylogenetic tree was estimated using the maximum likelihood method and a suitable parameter model with MEGA X [32].

2.5. Primer Design for Molecular Detection

The HCRSV isolates in the NCBI database were subjected to multiple sequence alignment (MSA) to determine the consensus regions among them. Forward and reverse primers were designed based on the consensus region. The MSA and primer designing was primarily done using the available online version of the software BioEdit version 7.7, OligoCalc, and PrimerBlast, which cover the filters for good primer design, such as suitable melting temperature, GC ratio, self-dimer, and hairpin formation [34,35]. Three primer pairs were designed based on the NCBI database's consensus sequence of all the HCRSV isolates reported and are listed in Table 2.

Table 2. Details of the primer pairs designed to be tested for molecular testing through RT-PCR amplification of the samples with the chlorotic spots symptom.

No.	Primer Name	Primer Sequence (5′–3′)	Expected Product Size	Target Region
1	HCRSV-Fwd-1	CCATTGCGAGTTTGTGGGC	421 bp	CP
	HCRSV-Rvs-1	CACATCCCCTTCAGATTGGC		
2	HCRSV-Fwd-2	CCAGTAGTTCCGACCCTAAGC	663 bp	CP
	HCRSV-Rvs-2	AGCCCACCCGAAGGATTTT		
3	HCRSV-Fwd-3	TGGCCACTCCTCTGGTACTTAC	947 bp	RdRp
	HCRSV-Rvs-3	CGCATCCACAGAAACGTGCTG		

Note: The primer design was sourced from information in the NCBI database. Fwd: forward primer; Rvs: reverse primer; bp: base pair (amplicon size); CP: coat protein; RdRp: RNA-dependent RNA polymerase.

2.6. cDNA Synthesis and RT-PCR

Synthesis of cDNA of the total RNA extracts was done using Thermo Scientific RevertAid First Strand cDNA Synthesis Kit (Universiti Kebangsaan Malaysia, Selangor, Malaysia) according to the manufacturer’s protocol; for each RNA extract, the template RNA (0.1 ng–5 ng) was added into a nuclease-free tube that was put on ice. Afterwards, the remaining components of the kit were added to the tube: 1 µL of Oligo (dT)18 primer, 4 µL of 5X Reaction Buffer, 1 µL of RiboLock RNase Inhibitor (20 U/µL), 2 µL of 10 mM dNTP Mix, 1 µL of RevertAid M-MuLV RT (200 U/µL), and nuclease-free water to the total volume of 20 µL. The content of the tube was mixed gently and briefly centrifuged. Then, the tube was incubated for 60 min at 42 °C and terminated by heating for 5 min at 70 °C. The tube containing the reaction product was then kept at –80 °C until used for PCR.

The PCR amplification was done using the Thermo Scientific DreamTaq PCR Master Mix (2×) Kit according to the manufacturer’s protocol: 25 µL of DreamTaq PCR Master Mix (2×) was put into a PCR tube on ice, then added with forward and reverse primer (0.1–1.0 µM each), the template cDNA product from earlier (10 pg – 1 µg), and nuclease-free water up to 50 µL total volume. The thermocycling conditions were as follows: initial denaturation for 30 s at 95 °C; 35 cycles of 10 s at 98 °C, 20 s at 56 °C, and 3 min at 72 °C; followed by a final extension of 10 min at 72 °C (BIORAD T100 Thermal Cycler, Universiti Kebangsaan Malaysia, Selangor, Malaysia). A negative control (no virus, symptomless sample) was included. Then, electrophoresis was performed by running 5 µL of the RT-PCR product onto the wells of 1% agarose gel with TAE buffer, which was stained with ethidium bromide. The visualisation of the expected band was done under UV light.

2.7. Light Microscopy

The symptomatic and symptomless (healthy) leaves were collected and brought to the anatomy laboratory in the Faculty of Science and Technology, UKM, Malaysia. The leaves’ transverse sections (around 30 µm)—namely, petiole, midrib, and lamina—were prepared from a fresh leaf held between polystyrene pieces by slicing using a sliding microtome (Leica SM2000 R, Universiti Kebangsaan Malaysia, Selangor, Malaysia). The sliced samples were separated into two groups. Those in the first group were mounted in distilled water for the initial observation under a light microscope (Olympus BX43, Universiti Kebangsaan Malaysia, Selangor, Malaysia), while those in the second group were preserved in sodium hypochlorite (Clorox) for 3 min before being washed with 3 changes of distilled water. Histochemical analysis of the samples (second group) was done via staining [36,37]. The samples were stained with both Safranin and Alcian blue stains for 15 min each before being washed with 3 changes of distilled water. Afterwards, samples were dehydrated with increasing ethanol concentrations (50%, 70%, 90%, 100%) for 5 min each. The samples were then transferred to a slide and mounted with Euparal. The photomicrographs of the sections were observed and taken using the light microscope (Olympus BX43) with the Analysis DoCu and EOS Utility 2 software.

2.8. Scanning Electron Microscopy

The samples were taken to the Electron Microscopy Unit, UKM, Malaysia, for preparation for the scanning electron microscope (SEM) [29]. The samples were cut into approximately 1 cm² sections along the leaf midrib. The sections were fixed in 4% glutaraldehyde overnight at 4 °C. The sections were then washed with 0.1 M phosphate buffer before being dehydrated in an acetone series (35%, 50%, 75%, 95%, and 100%) for 30 min each. Sections were then placed in a critical point drying machine for 30 min to let them dry. Afterwards, the sections were attached to the stub with double-sided tape. The sections were then coated using a sputter-coater machine (gold-coated) and observed via scanning electron microscope (LEO 1450-VP SEM).

The stomatal index (SI) is one of the best quantitative measurements of the anatomical characteristic of a plant. The SI is a percentage calculation that can be measured using the formula below:

$$SI = [s/(s + p)] \times 100 \quad (1)$$

where *s* is the number of stomata in view and *p* is the number of epidermal cells in the view.

3. Results

3.1. The Nucleotide Sequence of HCRSV-Malaysian Isolate

This study revealed that one contig (3873 bp) was present in the pooled sample after being aligned to the NCBI database using MegaBLAST [30]. The contig had the highest similarity (93.37%) with the HCRSV isolate from Singapore (GenBank accession number: NC_003608.1) with a typical genome organisation of the HCRSV containing seven putative ORFs (Figure 1). The revealed genome was deposited in GenBank with accession number MN080500.1 and named HCRSV-UKM.

Computational analysis done on the HCRSV-UKM genome revealed that it had a nucleotide similarity ranging from approximately 87 to 93% with the isolates from Singapore (NC_003608.1), USA (MT512573.1), Brazil (MK279671.1), China (KY933060.1), Israel (KC876666.1), and Taiwan (DQ392986.1) [7,15,21,38]. The highest nucleotide sequence similarity of HCRSV-UKM was with the HCRSV from Singapore (93.37%), while the lowest sequence similarity was with the HCRSV from Taiwan (87.90%) (Table 3). Figure 2 outlines the identity plot of the HCRSV isolates showing the general overview of their nucleotide sequence identity [7]. In addition to the nucleotide sequence similarity, the amino acid sequence could also be deduced and compared using the ORF prediction. Table 3 shows the comparison between the HCRSV isolates.

Table 3. Comparison of the percentage similarities of nucleotide and deduced amino acid sequences between the HCRSV-UKM and other HCRSV isolates available in NCBI GenBank.

HCRSV-UKM (MN080500.1)	HCRSV Isolate					
	Singapore (NC_003608.1)	TW_Taiwan (DQ392986.1)	XM_China (KY933060.1)	Is_Israel (KC876666.1)	SB01_Brazil (MK279671.1)	OUGC_USA (MT512573.1)
Nucleotide sequence (%)						
Complete genome	93.37	87.90	92.99	92.29	93.19	93.31
Predicted amino acid sequence by ORF (%)						
RdRp	96.32	90.15	94.82	95.91	96.19	95.78
P28	95.79	85.05	91.12	93.46	94.86	94.86
P23	82.74	69.42	80.00	80.71	81.22	85.79
P9	100.00	84.62	96.15	91.38	98.72	93.10
P8	91.43	87.14	97.14	97.14	98.57	92.86
P25	94.20	87.50	95.09	91.96	95.98	95.09
CP	96.52	95.94	97.97	93.62	97.68	97.10

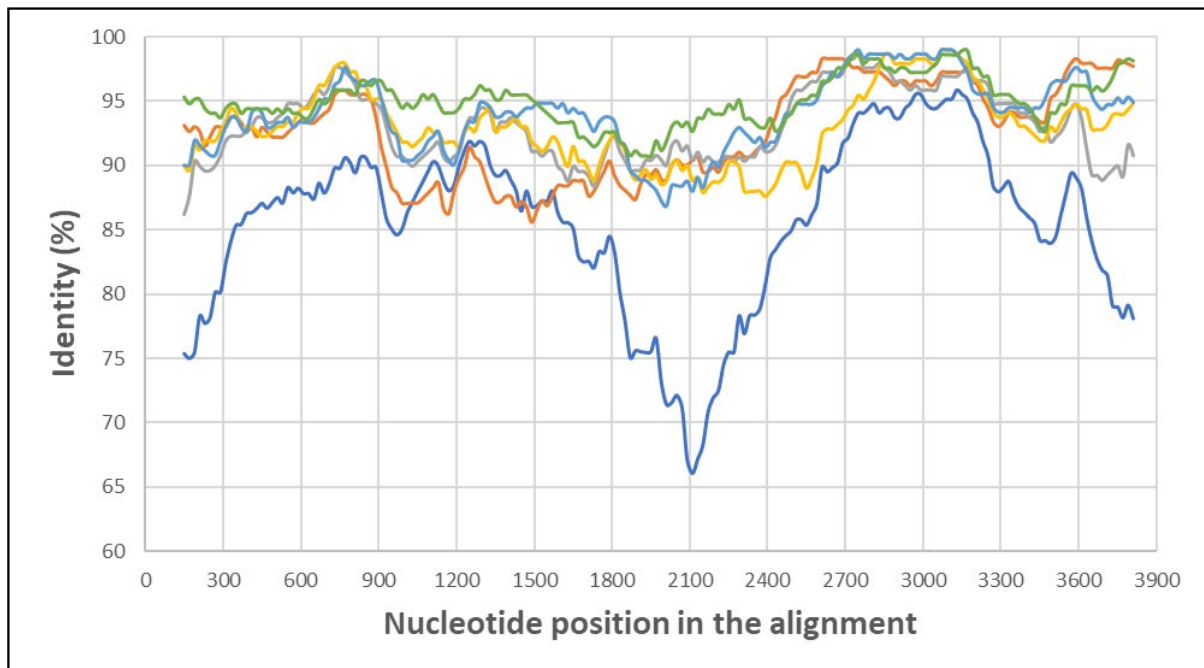


Figure 2. Nucleotide sequence identity similarity between the HCRSV isolates with the complete genome. The HCRSV from Singapore (NC_003608.1) was the reference genome for the species, and the remaining isolates can be seen in the figure (TW_Taiwan—dark blue line, UKM_Malaysia—orange line, XM_China—grey line, Is_Israel—yellow line, SB01_Brazil—light blue line, and OUGC_USA—green line). Data were generated using SimPlot software [31]. Window size: 300 nts, step size: 20 nts. This figure is adapted from the method developed by [7].

The predicted amino acid sequence of HCRSV-UKM showed varying degrees of similarity across all the other putative amino acids from other HCRSV isolates (Table 3). The putative *p23* had the lowest percentage of amino acid sequence similarity. All the predicted amino acid sequences were put through the motif scan tools at ExPASy-MyHits (https://myhits.isb-sib.ch/cgi-bin/motif_scan, accessed on 1 March 2023) [7]. The results of the motif scan show that the RdRp and CP both have the potential for the catalytic domain and shell (S) domain, respectively.

Maximum likelihood phylogenetic analysis based on the multiple sequence analysis of the complete genomes of *Betacarmoviruses* was performed with a bootstrapping of 1000 replications using the software MEGA X. Figure 3 shows the phylogenetic tree of the position of HCRSV-UKM (in red box) with the other six HCRSV isolates and other *Betacarmoviruses*.

3.2. Detection of the HCRSV Using RT-PCR

RT-PCR was utilised as a complementary method alongside the RNA-Seq to confirm the presence of the HCRSV in *H. rosa-sinensis* in Malaysia. The designed primer pairs (Table 2) were used for the molecular detection of the HCRSV. RT-PCR products were generated from the symptomatic leaves of *H. rosa-sinensis* from different landscape plantings' locations, with varying degrees of positive tests, as can be examined in Figures 4 and 5. All three primer pairs had more than 50% efficacy for the diagnostics of the symptomatic samples, with around 52% for HCRSV-Fwd-Rvs-1 (primer pair 1), 84% for HCRSV-Fwd-Rvs-2 (primer pair 2), and 81% for HCRSV-Fwd-Rvs-3 (primer pair 3). A symptomless sample was collected and tested, showing no bands.

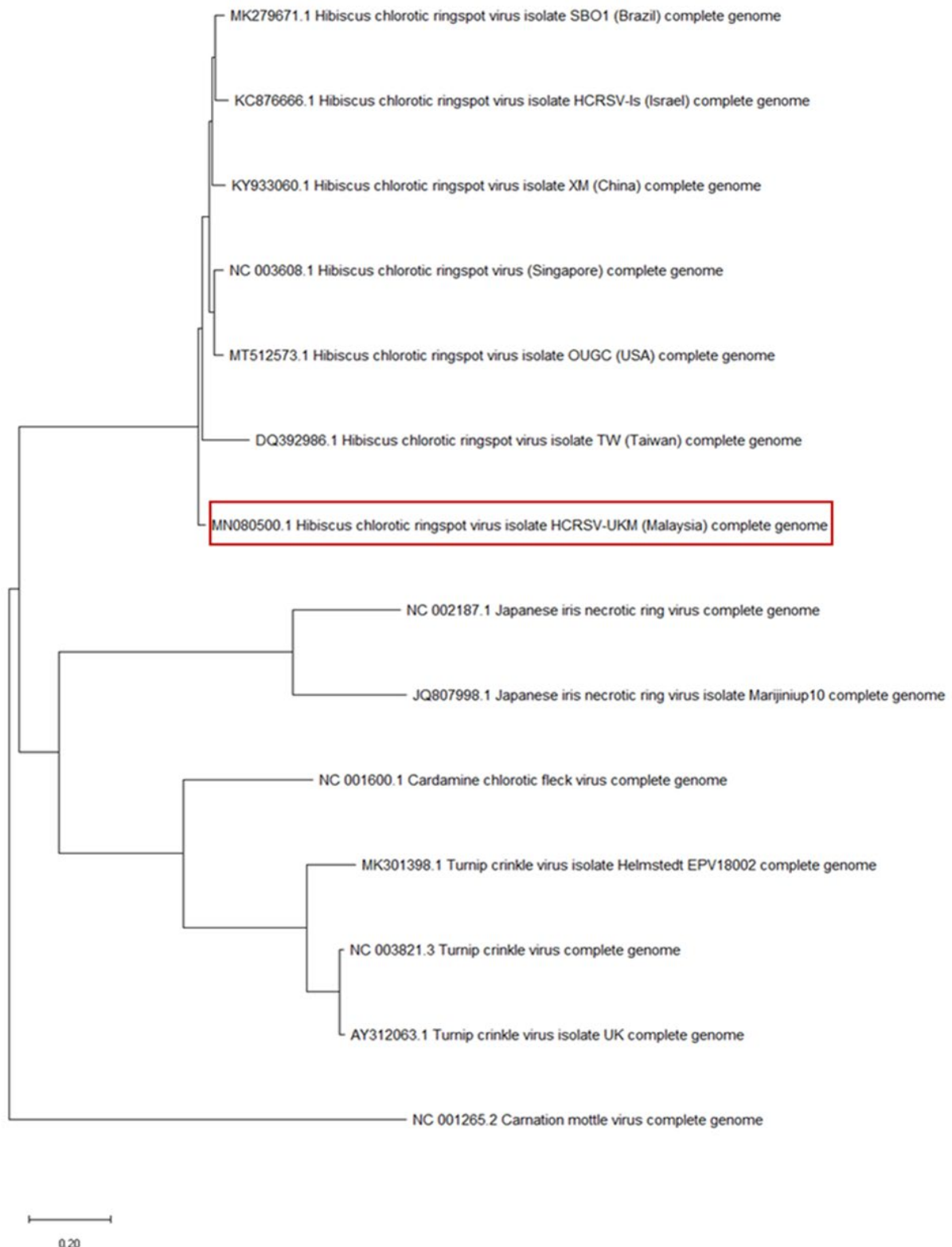


Figure 3. The evolutionary history was inferred using the maximum likelihood method and general time reversible model conducted using MEGA X. Phylogenetic tree generated from multiple sequence alignment of the complete genomes of viruses from the NCBI GenBank, showing the position of the revealed genome of this study, HCRSV-UKM (in red box), among Betacarmoviruses. Carnation mottle virus (NC_001265.2) was used as the outgroup. The tree shows the accession number and the name of the respective virus. Scale bar represents a genetic distance of 0.2.

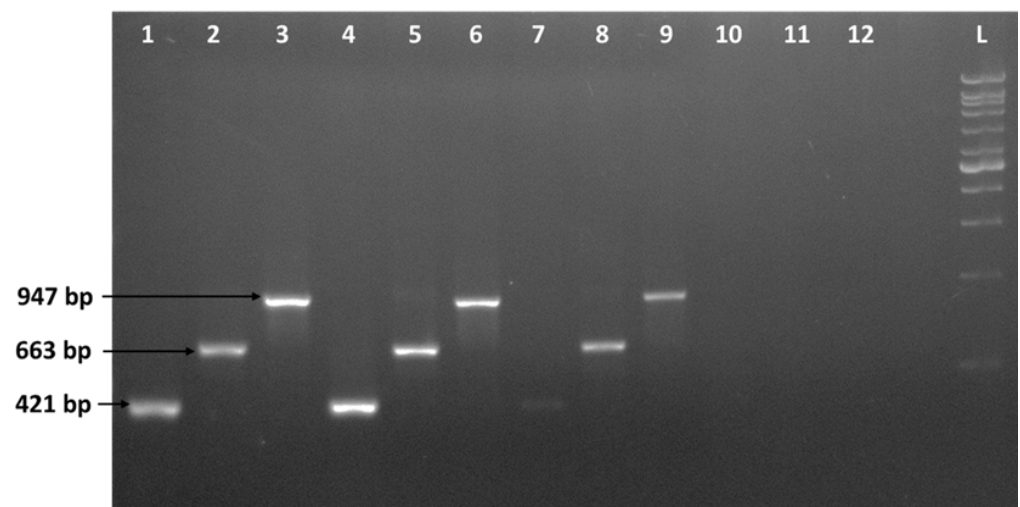


Figure 4. Detection of Hibiscus chlorotic ringspot virus in leaves of *H. rosa-sinensis* in different landscape plantings using RT-PCR. The figure shows the result of several samples. 1, 2, and 3: Bangi samples using primer pairs 1, 2, and 3, respectively. 4, 5, and 6: Putrajaya samples using primer pairs 1, 2, and 3, respectively. 7, 8, and 9: Ipoh samples using primer pairs 1, 2, and 3, respectively. 10, 11, and 12: control for each primer pair. L: VC 1 kb DNA ladder.

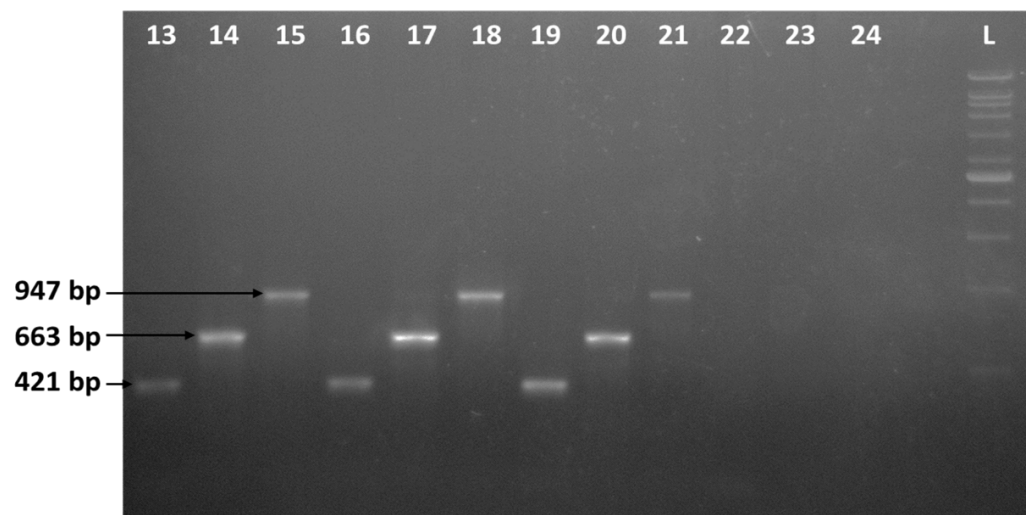


Figure 5. Detection of Hibiscus chlorotic ringspot virus in leaves of *H. rosa-sinensis* in different landscape plantings using RT-PCR. The figure shows the result of several samples. 13, 14, and 15: UKM samples using primer pairs 1, 2, and 3, respectively. 16, 17, and 18: Nilai samples using primer pairs 1, 2, and 3, respectively. 19, 20, and 21: Raub samples using primer pairs 1, 2, and 3, respectively. 22, 23, and 24: control for each primer pair. L: VC 1 kb DNA ladder.

3.3. Anatomical and Morphological Analysis of the *H. rosa-sinensis* Leaf

Changes to the leaf structure of infected *H. rosa-sinensis* were examined and compared with the healthy leaf sample (Figures 6 and 7). The transverse sections of the leaf lamina, petiole, and midrib were observed under a light microscope. The micromorphological characteristics of the samples were observed under a scanning electron microscope (SEM). This study found that there were indeed several differences in the characteristics of the samples that could be used to differentiate an infected individual plant.

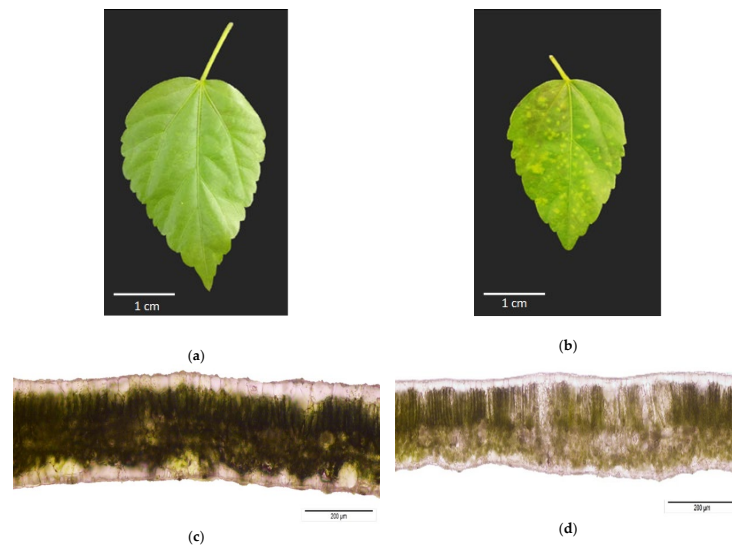


Figure 6. The leaves of *H. rosa-sinensis*. (a) The healthy leaf showing no symptoms. (b) Symptomatic leaf showing chlorotic spots. (c) Transverse sections of the healthy leaf lamina with thick chlorophyll distribution (arrow). (d) Transverse sections of the symptomatic leaf lamina with uneven chlorophyll distribution (arrow).

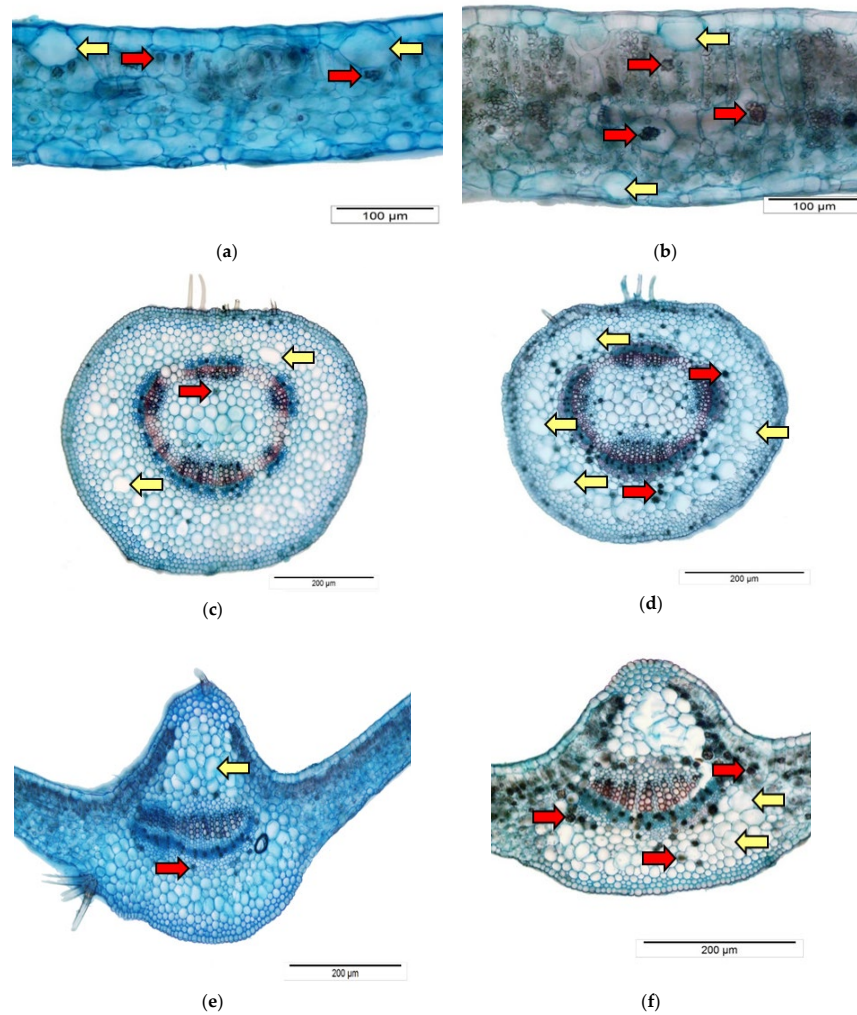


Figure 7. Transverse sections of leaf lamina, petiole, and midrib of *H. rosa-sinensis*. (a,c,e) show the healthy leaf sample, while (b,d,f) show the HCRSV-infected leaf sample. Red arrows point at druses, while yellow arrows point at mucilaginous idioblast cells. (a) Leaf lamina of a healthy leaf showing

the druses and mucilaginous idioblast cells. (b) Leaf lamina of an HCRSV-infected leaf showing the druses and mucilaginous idioblast cells. (c) Petiole of a healthy leaf sample. (d) Petiole of an HCRSV-infected leaf sample. (e) The midrib of a healthy leaf sample. (f) The midrib of an HCRSV-infected leaf sample.

3.3.1. Transverse Sections of the Leaf Lamina

The transverse sections of the leaf lamina, petiole, and midrib of healthy and HCRSV-infected samples are presented in Figure 7. Generally, there were changes observed in the transverse sections of the leaf of the infected sample compared with the healthy one: certain characteristics were reduced while others appeared to be increased.

In the leaf lamina, the chlorophyll distribution in the healthy sample was abundant and arranged neatly throughout. Meanwhile, the chlorophyll distribution in the infected sample was reduced and scattered on the region with the infection symptom (chlorotic spots). The average diameter for the leaf lamina in the infected sample increased by approximately 79.12% compared with the healthy sample. The average height of the epidermis in the infected sample also increased by around 6.22%. The average width of the epidermis in the infected sample also increased by around 77.64%. The chlorenchyma in both healthy and infected samples consisted of one layer of the palisade, but different layers of the spongy mesophyll, with 4–6 layers and 2–5 layers, respectively. Mucilaginous idioblast cells could be observed in the epidermis in both samples. There were druses observed in the chlorenchyma in both samples.

3.3.2. Transverse Sections of the Petiole

For the petiole anatomical characteristics in Figure 7, observation of petiole transverse sections showed that the average diameter of the infected sample was thicker compared with the healthy one by approximately 5.88%. The average height of the epidermis of the infected sample was shorter than the healthy one by approximately 5.23%, and the average width of the epidermis of the infected sample was smaller than the healthy sample by approximately 8.04%. Meanwhile, the hypodermis of the infected sample had a shorter average height compared with the healthy sample by approximately 2.79%, while the average width was smaller by approximately 1.09%. The cortex observed in the infected sample had 6–8 layers of parenchyma cells, while the healthy sample had 5–7 layers of parenchyma. The diameter of the parenchyma in the infected sample was reduced by approximately 44.31% compared with the healthy sample. Both infected and healthy samples had a closed vascular bundle. The average diameter of both the xylem and phloem in the infected sample was larger compared with the healthy sample by approximately 73.67% and 16.56%, respectively. Sclerenchyma cells were only observed in the infected sample, just outside the vascular bundle. The mucilaginous idioblast cells were observed in both the infected and healthy samples. The druses could also be observed throughout both infected and healthy samples. The average diameter of the pith of the infected sample was slightly smaller than the healthy sample by approximately 6.06%. Simple trichomes were observed on the adaxial side of both the infected and healthy samples. Glandular trichomes were only observed on the abaxial side of the healthy sample.

3.3.3. Transverse Sections of the Midrib

For the midrib anatomical characteristics, the average diameter of the infected sample was reduced compared with the healthy sample by approximately 17.86%. The average height of the epidermis of the infected sample increased by 19.78%, while the average width of the epidermis of the infected sample also increased by 27.45%. For the palisade, the average height and width in the infected sample increased by 99.17% and 89.39%, respectively, compared with the healthy one. The diameter of the collenchyma cells in the infected sample was reduced by approximately 25.25% compared with the healthy sample. Trichomes were observed only in the healthy sample. An opened system of the vascular

bundle was observed in both samples, with the average diameter of the xylem thickened in the infected sample by 34.07%. Meanwhile, the average diameter of the phloem in the infected sample was also a little bit thicker compared with the healthy one by around 2.79%. Sclerenchyma cells were only observed in the infected sample. Mucilaginous idioblast cells and druses could be found in both samples.

3.3.4. Micromorphological Analysis of the Leaf Lamina of *H. rosa-sinensis*

The micromorphological analysis was done on the leaf of *H. rosa-sinensis* by comparing the infected and healthy samples via observation under an SEM (Figure 8). Like the anatomical analysis, the morphological study showed that certain characteristics were different, and others were similar between the healthy and infected samples.

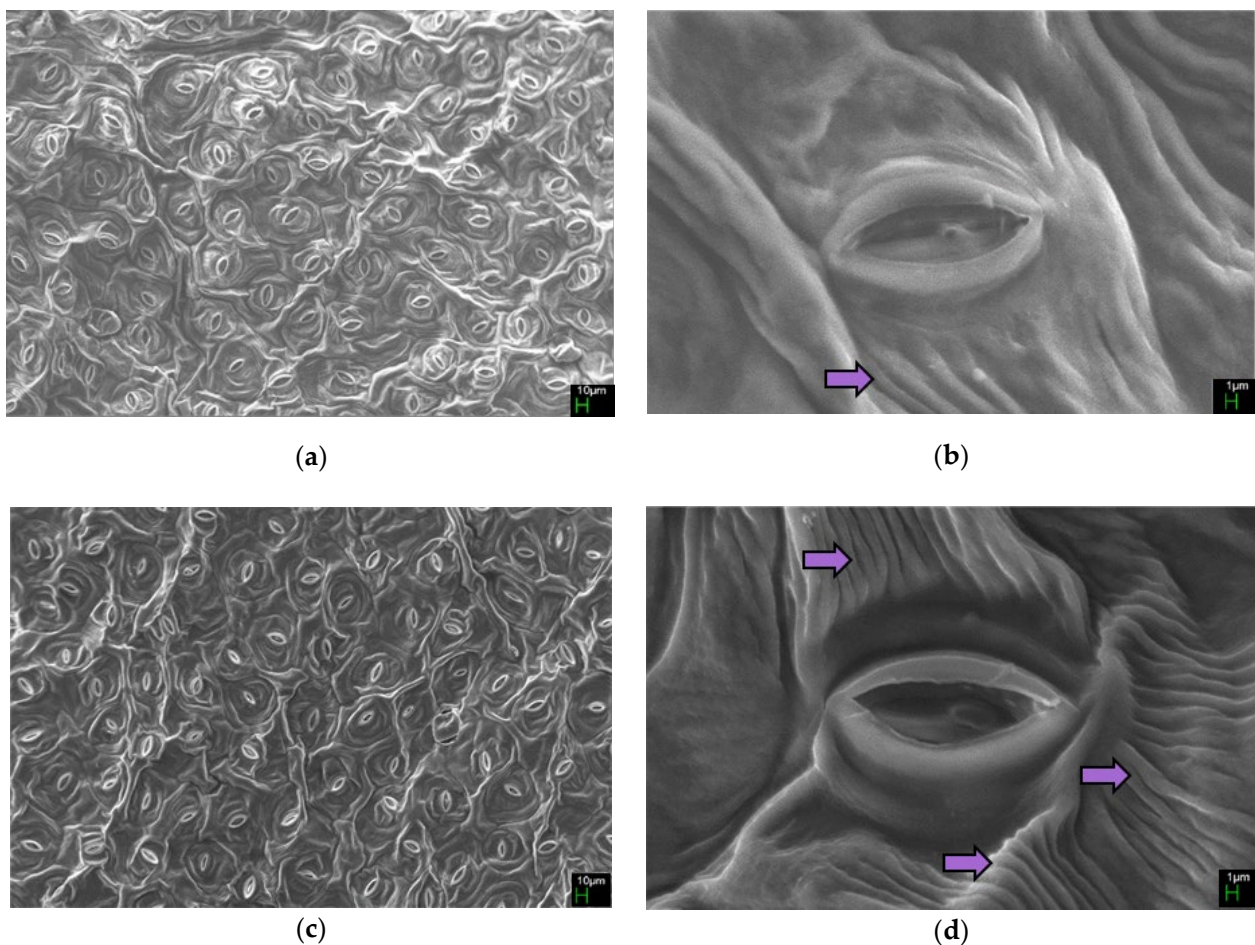


Figure 8. The micrograph under an SEM of the *H. rosa-sinensis* leaf epidermis. (a,b) are from the healthy leaf sample, while (c,d) are from an HCRSV-infected leaf sample. Purple arrows point at cuticular ornamentation. (a,c) The structure of anticlinal and periclinal walls surrounding trichomes and stomata can be observed on the epidermis of the leaf abaxial leaf surface. (b) Hypostomatic stomata with striae cuticular ornamentation (purple arrow). (d) Hypostomatic stomata with increased striae cuticular ornamentation compared with the healthy leaf sample (purple arrow).

In both samples, there was clear abaxial epidermis cuticle ornamentation, where the anticlinal walls merged to form a ridge, whereas the periclinal walls subsided to form cleavage. There was also clear ornamentation on the adaxial side, where the anticlinal walls merged to form a ridge and the periclinal walls subsided to form cleavage. Cuticles on the adaxial epidermis surface in both samples were observed. In both samples, the cuticles on the leaf abaxial epidermis surface were clearer surrounding the stomata. However, the cuticle linings were more pronounced in the infected sample compared with the healthy

one. In both samples, hypostomatic stomata were found randomly scattered on the abaxial side of the leaf epidermis, in which the infected sample exhibited a reduced average of the length and width of the stomata by approximately 12.41% and 3.03%, respectively. Furthermore, the stomatal index of the infected sample was higher at 44.7% compared with the healthy sample at 28.2%.

4. Discussion

The phylogenetic tree that was generated showed that the identity and classification of the discovered genome were indeed the HCRSV [11]. The phylogenetic analysis of the HCRSV-UKM (Malaysian isolate) revealed an approximately 87–93% sequence similarity with the other six isolates—namely, from Singapore, USA, Brazil, China, Israel, and Taiwan—recorded in the NCBI database. Additionally, the predicted amino acid sequence of all seven ORFs of HCRSV-UKM revealed between 69–100% sequence similarity with the other six isolates. While the sequence similarity differed between the isolates, the percentage was still within an acceptable range to still be classified as the same species [39]. The chlorotic spot symptom found in Malaysian *H. rosa-sinensis* was in line with previous reports and studies [6,7,12,18,19,21,23].

Adopting a molecular approach has been the standard for the detection of viral presence in plant populations, with RT-PCR being one of the widely used methods [40]. RT-PCR was shown to be efficient at detecting viruses in plants, making it a robust strategy for screening imported material and quarantining infected samples [40–42]. This study utilised RT-PCR as a complementary molecular technique to RNA sequencing to successfully confirm the presence of the HCRSV in *H. rosa-sinensis* in Malaysia. To our knowledge, this study was the first to use RT-PCR to investigate the presence of the virus in Malaysian *H. rosa-sinensis*. Apart from characterising the virus symptom and infection on the host species, a molecular detection strategy is essential in addressing the issue of plant viral infection. There is a need for this entire study to be done to gather the necessary information considering the potential for the host plant to act as a virus reservoir that could cause serious damage to other plants [10,43].

Microscopy was used to examine the anatomical structures of healthy and infected leaves, such as chloroplasts. The chloroplasts in the infected sample (with symptom chlorosis) were reduced compared with the healthy one. This agreed with previous studies that recorded lower amounts and smaller sizes of chloroplasts, palisade, and spongy mesophyll cells in virus-infected samples compared with their healthy counterparts [44–46]. Unsurprisingly, the chlorophyll distribution in the healthy sample was significantly higher compared with the infected samples. It was observed that the healthy sample contained a thick, healthy amount of chlorophyll pigmentation compared with the infected one. This showed that viral infection could lead to a reduction in chlorophyll, which then could negatively affect the photosynthetic pathways in plants [47]. Interestingly, the chloroplast is a target for the plant viral infection cycle, but at the same time, could potentially have a role in plant defence [48,49]. Further studies on the impact of viruses on the chlorophyll distribution in *H. rosa-sinensis* would be beneficial to properly examine the plant cell–virus interaction in this host. [47,48].

The transverse section of petioles showed differences between healthy and infected samples. Apart from the taxonomic importance, the anatomical characteristics can be regarded as plant adaptations against viral infections [50]. One of the adaptations is the presence of trichomes. Overall, the number of trichomes in the healthy sample was fewer compared with the infected samples. This is in line with a previous study suggesting the number of trichomes corresponding to the defence against pathogen infestation due to its containing chemical protectants for the plant [51]. Trichome formations were also suggested to cause developmental stress on plant growth yet are essential for plant protection against pathogens and even predators [52].

Another adaptation is the relative size of the epidermis layer between healthy and infected samples. The result shows that the infected samples had a thicker epidermis

compared with the healthy sample. These data were in keeping with a previous publication that mentioned the possibility of a thick epidermis providing a leaf texture acting as protection that could at least partially hinder virus penetration into the plant cells, insect vectors, and mechanical shocks [53].

The phloem and xylem of the healthy sample were smaller compared with the infected one. This coincided with previous studies on the structural changes that occur in virus-infected plants [44,46]. However, the molecular mechanisms that influence viral infection and cell size are yet to be fully understood. The vascular bundle was related to the systemic plant virus movement. Interestingly, the living state of the phloem makes it the most studied means of virus transport compared with the non-living state of the xylem, although both could, to a certain extent, carry virus particles [54]. It remains challenging to study a sample of vascular tissues due to the ease of contamination. As such, studying the associated proteins has become the preferred method to understand the plant response against viral infection, where phloem-associated defence and signalling protein genes can be detected upon viral infestation [54].

Sclerenchyma is an elastic support system made up of a collection of cells with lignified walls that strengthen the overall tissue of plants [55]. This group of cells was present only in the HCRSV-infected samples, which may be important as an adaptation to provide strength to the plant against environmental stress [56].

Mucilage or mucilaginous idioblast cells were found to be abundant in the infected sample compared with the healthy sample. Mucilage is a cell containing beneficial secretions of secondary metabolites [55,57]. While it is intriguing to claim that the cells are an adaptation against plant viruses, there is yet a study that specifies the mechanism of the mucilage cells.

Druse is a form of calcium oxalate crystals that can be observed in plant cells and was found to act as a deterrent against insects and even as a source of carbon dioxide [58,59]. In many cases, the presence of druse was linked to the plant's adaptation to stresses to ensure its survival. Relatively speaking, the distribution of druse in the healthy sample was low in the pith, parenchyma cortex, hypodermis, and collenchyma, but high in the vascular tissue. In the HCRSV-infected sample, the distribution of druse was relatively very high in the pith, parenchyma cortex of petiole, and collenchyma; and the distribution of druse is high in the hypodermis, palisade, parenchyma cortex of midrib, and the vascular tissue. Overall, all samples contained druses, but relatively more in the infected sample compared with the healthy one. These data suggest that the plant is always prepared for defence using calcium oxalate and will increase the production of the mineral in case of a viral attack [60].

A characteristic that was observed through the SEM was the cuticle. The cuticle is a waxy layer on the outermost part of the epidermis. The structure is widely known as the protective layer that reduces the rate of water loss from the leaf surface and also as a defence mechanism [55]. Studies were done that explored its role in plant defence against extreme environmental stresses, mechanical injuries, and pathogen infestations [61]. The observation of the samples showed that the formation of the cuticle on the HCRSV-infected and healthy samples was similar. The anticlinal and periclinal walls could be observed in both healthy and HCRSV-infected samples. However, the cuticle linings were mostly observed in the HCRSV-infected sample compared with the healthy sample. These 'cuticle linings' are also referred to as 'striae' [62]. Plant cuticle has the potential for an essential role in plant-pathogen interactions, where it is involved as a defence signalling factor that contributes to the pathways to promote defence [61]. It is worth mentioning that cuticle studies remain elusive, and the cuticle is yet to be understood fully, especially concerning the data found in this study.

Another significant anatomical characteristic is the stomata. This structure is widely recognised as the 'pair of guard cells' for gaseous exchange and plant transpiration. Like cuticles, stomata were also studied for their potential in plant defence against pathogens [63]. From the data, stomata observed in the healthy sample were larger compared with the HCRSV-infected sample. The smaller size of the infected sample would reduce the number

of openings available for pathogen entry, as this is the most straightforward adaptation for plant defence [63]. However, this adaptation could reduce plant tolerance against environmental stresses that are dependent on the openings of the stomata [64].

The stomatal index (SI) of a plant could be influenced by the amount of light, carbon dioxide concentration, and humidity of the surroundings [52]. The data showed that the SI of the healthy sample was lower (28.2%) compared with the HCRSV-infected sample (44.7%). It is also interesting to consider that these data are in line with [52], where the plants with lower SI have fewer trichomes, potentially due to the environmental adaptation of the plant species.

Other factors that should be considered are the incubation period (time between pathogen infection and symptom expression) and the latent period (time between host infection and the onset of pathogen infectiousness from that infection) [65]. These two periods are essential in managing the epidemics of plant pathogens and could also be affecting the variance in symptoms exhibition in the host and the anatomical adaptations, although more studies must be done to confirm this [66,67].

5. Conclusions

This study established that *H. rosa-sinensis* in Malaysia is a host species for the plant virus HCRSV. The leaves of the host plant exhibited the chlorotic spots symptom. This was the first report on the complete genome of the HCRSV found infecting *H. rosa-sinensis* in Malaysia.

The phylogenetic analysis elucidated the sequence similarity of the HCRSV found in Malaysia to the other isolates found in *H. rosa-sinensis* in different parts of the world. The molecular approach used in this research validated the viability of RT-PCR as a suitable detection tool for diagnosing viruses infecting plants in Malaysia, allowing for better control of the spread into and throughout the country. The anatomical and micromorphological analysis of *H. rosa-sinensis* in this study showed the adaptations of the plant leaf structure as a response to pathogen infection. Understanding the formation of these structures as an adaptation could help to further the knowledge regarding plant viral mechanisms and defence. This could lead to a better understanding of the severity of infection, thus highlighting the importance of protecting the host plant species.

In conclusion, this study demonstrated the presence of HCRSV infection in *H. rosa-sinensis* within the geographical range in Malaysia, the complete genome of the HCRSV isolate, a reliable molecular detection method, and its impact on the host anatomy and morphology. These results shall help to formulate a management strategy to better protect the Malaysian national flower.

Author Contributions: Conceptualisation, N.T. and H.B.; methodology, M.S.M.Y., N.L., N.T. and H.B.; software, M.S.M.Y. and S.H.; validation, N.T., M.F.M.S., A.A., M.N.S., H.S.H., S.H. and H.B.; formal analysis, M.S.M.Y. and N.L.; investigation, M.S.M.Y., N.L. and M.F.M.S.; resources, N.T., A.A., S.H. and H.B.; data curation, M.S.M.Y., N.L. and M.F.M.S.; writing—original draft preparation, M.S.M.Y. and N.L.; writing—review and editing, N.T., M.F.M.S., A.A., M.N.S., H.S.H., S.H. and H.B.; visualisation, M.S.M.Y. and N.L.; supervision, N.T., S.H. and H.B.; project administration, M.F.M.S., A.A., M.N.S., H.S.H., S.H. and H.B.; funding acquisition, H.B. All authors read and agreed to the published version of the manuscript.

Funding: This research was supported by Universiti Kebangsaan Malaysia (DIP-2020-019 and SK-2022-015).

Data Availability Statement: The complete genome sequence in this study, namely, HCRSV-UKM, was deposited in GenBank under the accession number MN080500.1.

Conflicts of Interest: The authors declare no conflict of interest.

References

1. Afiune, L.A.F.; Leal-Silva, T.; Sinzato, Y.K.; Moraes-Souza, R.Q.; Soares, T.S.; Campos, K.E.; Fujiwara, R.T.; Herrera, E.; Damasceno, D.C.; Volpato, G.T. Beneficial effects of *Hibiscus rosa-sinensis* L. flower aqueous extract in pregnant rats with diabetes. *PLoS ONE* **2017**, *12*, e0179785. [[CrossRef](#)] [[PubMed](#)]
2. Ganesan, S.; Sabran, S.F.; Mazlun, M.H. Plant Diversity Assessment and Traditional Knowledge Documentation of Home Gardens in Parit Raja, Batu Pahat, Johor. In Proceedings of the IOP Conference Series: Earth and Environmental Science, Moscow, Russia, 27 May–6 June 2019; Volume 269.
3. Khan, I.M.; Rahman, R.; Mushtaq, A.; Rezgui, M. *Hibiscus rosa-sinensis* L. (Malvaceae): Distribution, Chemistry and Uses. *Int. J. Chem. Biochem. Sci.* **2017**, *12*, 147–151.
4. Khristi, V.; Patel, V.H. Therapeutic Potential of *Hibiscus rosa-sinensis*: A Review. *Int. J. Nutr. Diet.* **2016**, *4*, 105–123. [[CrossRef](#)]
5. Missoum, A. An update review on *Hibiscus rosa sinensis* phytochemistry and medicinal uses. *J. Ayurvedic Herb. Med.* **2018**, *4*, 135–146. [[CrossRef](#)]
6. Pourrahim, R.; Ghobakhlo, A.; Farzadfar, S. Biological and molecular detection of Hibiscus chlorotic ringspot virus infecting *Hibiscus rosa-sinensis* in Iran. *Phytopathol. Mediterr.* **2013**, *52*, 528–531. [[CrossRef](#)]
7. Ramos-González, P.L.; da Costa-Rodrigues, M.; Potsclam-Barro, M.; Chabi-Jesus, C.; Banguela-Castillo, A.; Harakava, R.; Kitajima, E.W.; Freitas-Astúa, J. First genome sequence of an isolate of hibiscus chlorotic ringspot virus from the Western hemisphere. *Trop. Plant Pathol.* **2020**, *45*, 153–158. [[CrossRef](#)]
8. Brunt, A.A.; Barton, R.J.; Phillips, S.; Lana, A.O. Hibiscus latent ringspot virus, a newly recognised virus from *Hibiscus rosa-sinensis* (Malvaceae) in western Nigeria. *Ann. Appl. Biol.* **1980**, *96*, 37–43. [[CrossRef](#)]
9. Adkins, S.; Kamenova, I.; Chiemsombat, P.; Baker, C.A.; Lewandowski, D.J. Tobamoviruses from hibiscus in Florida and beyond. *Acta Hortic.* **2006**, *722*, 65–70. [[CrossRef](#)]
10. Kitajima, E.W.; Rodrigues, J.C.V.; Freitas-Astua, J. An annotated list of ornamentals naturally found infected by Brevipalpus mite-transmitted viruses. *Sci. Agric.* **2010**, *67*, 348–371. [[CrossRef](#)]
11. Srinivasan, K.G.; Narendrakumar, R.; Wong, S.M. Hibiscus virus S is a new subgroup II tobamovirus: Evidence from its unique coat protein and movement protein sequences. *Arch. Virol.* **2002**, *147*, 1585–1598. [[CrossRef](#)]
12. Waterworth, H.E.; Lawson, R.H.; Monroe, R.L. Purification and Properties of Hibiscus Chlorotic Ringspot Virus. *Phytopathology* **1976**, *66*, 570–575. [[CrossRef](#)]
13. Mitrofanova, I.V.; Zakubanskiy, A.V.; Mitrofanova, O.V. Viruses infecting main ornamental plants: An overview. *Ornam. Hortic.* **2018**, *24*, 95–102. [[CrossRef](#)]
14. Singh, B.P.; Srivastava, K.M.; Raizada, R.K. Viruses of Ornamental—Identification and Diagnosis. In *Horticulture—New Technologies and Applications*; Springer: Dordrecht, The Netherlands, 1991; pp. 321–328, ISBN 978-94-011-3176-6.
15. Huang, M.; Koh, D.C.; Weng, L.J.; Chang, M.L.; Yap, Y.K.; Zhang, L.; Wong, S.M. Complete nucleotide sequence and genome organization of hibiscus chlorotic ringspot virus, a new member of the genus Carmovirus: Evidence for the presence and expression of two novel open reading frames. *J. Virol.* **2000**, *74*, 3149–3155. [[CrossRef](#)]
16. Jones, D.R.; Behncken, G.M. Hibiscus Chlorotic Ringspot, a Widespread Virus Disease in the Ornamental *Hibiscus rosa-sinensis*. *Australas. Plant Pathol.* **1980**, *9*, 4–5. [[CrossRef](#)]
17. Koh, D.C.-Y.C.-Y.; Liu, D.X.; Wong, S.-M.S.-M. A Six-Nucleotide Segment within the 3' Untranslated Region of Hibiscus Chlorotic Ringspot Virus Plays an Essential Role in Translational Enhancement. *J. Virol.* **2002**, *76*, 1144–1153. [[CrossRef](#)]
18. Abdul-Samad, N.; Mat, M. Hibiscus Chlorotic Ringspot Virus in Malaysian Hibiscus. *Plant Dis. Note* **1995**, *79*, 967. [[CrossRef](#)]
19. Karanfil, A.; Korkmaz, S. First report of Hibiscus chlorotic ringspot virus in Turkey. *New Dis. Rep.* **2017**, *35*, 22. [[CrossRef](#)]
20. Li, S.C.; Chang, Y.C. First report of Hibiscus chlorotic ringspot virus in Taiwan. *Plant Pathol.* **2002**, *51*, 803. [[CrossRef](#)]
21. Luria, N.; Reingold, V.; Lachman, O.; Dombrovsky, A. Full-Genome Sequence of Hibiscus Chlorotic Ringspot Virus from Israel. *Genome Announc.* **2013**, *1*, 3155. [[CrossRef](#)]
22. Ong, J.W.L.; Li, H.; Sivasithamparam, K.; Dixon, K.W.; Jones, M.G.K.; Wylie, S.J. Novel and divergent viruses associated with Australian orchid-fungus symbioses. *Virus Res.* **2018**, *244*, 276–283. [[CrossRef](#)]
23. Tomassoli, L.; Mangli, A.; Tiberini, A.; Adkins, S. Investigation on the Phytosanitary Status of Major Ornamental Hibiscus Species in Italy to Assess Virus Infection. In Proceedings of the XIII International Symposium on Virus Diseases of Ornamental Plants, Oslo, Norway, 24–29 June 2015; ISHS: Leuven, Belgium, 2015; pp. 29–36.
24. Zhou, T.; Fan, Z.F.; Li, H.F.; Wong, S.M. Hibiscus chlorotic ringspot virus p27 and Its Isoforms Affect Symptom Expression and Potentiate Virus Movement in Kenaf (*Hibiscus cannabinus* L.). *Mol. Plant-Microbe Interact.* **2006**, *19*, 948–957. [[CrossRef](#)]
25. Liang, X.-Z.; Lucy, A.P.; Ding, S.-W.; Wong, S.-M. The p23 Protein of Hibiscus Chlorotic Ringspot Virus Is Indispensable for Host-Specific Replication. *J. Virol.* **2002**, *76*, 12312–12319. [[CrossRef](#)] [[PubMed](#)]
26. Zhang, X.; Wong, S.M. Hibiscus chlorotic ringspot virus upregulates plant sulfite oxidase transcripts and increases sulfate levels in kenaf (*Hibiscus cannabinus* L.). *J. Gen. Virol.* **2009**, *90*, 3042–3050. [[CrossRef](#)] [[PubMed](#)]
27. Meng, C.; Chen, J.; Ding, S.W.; Peng, J.; Wong, S.M. Hibiscus chlorotic ringspot virus coat protein inhibits trans-acting small interfering RNA biogenesis in Arabidopsis. *J. Gen. Virol.* **2008**, *89*, 2349–2358. [[CrossRef](#)] [[PubMed](#)]
28. Niu, S.; Gil-Salas, F.M.; Tewary, S.K.; Samales, A.K.; Johnson, J.; Swaminathan, K.; Wong, S.M. Hibiscus chlorotic ringspot virus coat protein is essential for cell-to-cell and long-distance movement but not for viral RNA replication. *PLoS ONE* **2014**, *9*, e113347. [[CrossRef](#)]

29. Manching, H.C.; Carlson, K.; Kosowsky, S.; Smitherman, C.T.; Stapleton, A.E. Maize Phyllosphere Microbial Community Niche Development Across Stages of Host Leaf Growth. *F1000Research* **2018**, *6*, 33. [[CrossRef](#)]
30. Haas, B.J.; Papanicolaou, A.; Yassour, M.; Grabherr, M.; Blood, P.D.; Bowden, J.; Couger, M.B.; Eccles, D.; Li, B.; Lieber, M.; et al. De novo transcript sequence reconstruction from RNA-seq using the Trinity platform for reference generation and analysis. *Nat. Protoc.* **2013**, *8*, 1494–1512. [[CrossRef](#)]
31. Lole, K.S.; Bollinger, R.C.; Paranjape, R.S.; Gadkari, D.; Kulkarni, S.S.; Novak, N.G.; Ingersoll, R.; Sheppard, H.W.; Ray, S.C. Full-Length Human Immunodeficiency Virus Type 1 Genomes from Subtype C-Infected Seroconverters in India, with Evidence of Intersubtype Recombination. *J. Virol.* **1999**, *73*, 152–160. [[CrossRef](#)]
32. Hall, B.G. Building phylogenetic trees from molecular data with MEGA. *Mol. Biol. Evol.* **2013**, *30*, 1229–1235. [[CrossRef](#)]
33. Kumar, S.; Stecher, G.; Li, M.; Niyaz, C.; Tamura, K. MEGA X: Molecular evolutionary genetics analysis across computing platforms. *Mol. Biol. Evol.* **2018**, *35*, 1547–1549. [[CrossRef](#)]
34. Hall, T.; Bioinformatics, I.; Carlsbad, C. BioEdit: An important software for molecular biology. *GERF Bull. Biosci.* **2011**, *2*, 60–61. [[CrossRef](#)]
35. Nugroho, I.B.; Handayani, N.S.N. Primer design and in silico analysis using CLUSTALW and MUSCLE for L-arabinose isomerase (araA) gene detection in thermophilic bacteria. In Proceedings of the AIP Conference Proceedings, Yogyakarta, Indonesia, 11–13 November 2015; AIP Publishing: New York, NY, USA, 2016; Volume 1755. [[CrossRef](#)]
36. Retamales, H.A.; Scharaschkin, T. A Staining Protocol for Identifying Secondary Compounds in Myrtaceae. *Appl. Plant Sci.* **2014**, *2*, 1400063. [[CrossRef](#)]
37. Shokefun, E.O.; Ayodele, A.E.; Akinloye, A.J. Systematic Importance of Leaf Anatomical Characters in Some Species of Microcos Linn. Section Eumicrocos Burret. in Nigeria. *Am. J. Plant Sci.* **2016**, *07*, 108–117. [[CrossRef](#)]
38. Olmedo-Velarde, A.; Hu, J.; Melzer, M.J. A Virus Infecting *Hibiscus rosa-sinensis* Represents an Evolutionary Link between Cileviruses and Higreviruses. *Front. Microbiol.* **2021**, *12*, 660237. [[CrossRef](#)] [[PubMed](#)]
39. International Committee on Taxonomy of Viruses. *Chapter Version: ICTV Ninth Report: Tombusviridae*; ICTV: San Diego, CA, USA, 2011.
40. Wang, J.; Li, W.; Cui, J.; Chen, X. The status of quarantine regulation on plant virus and its challenges. *J. Plant Sci.* **2020**, *4*, 194–198. [[CrossRef](#)]
41. Kinoti, W.M.; Nancarrow, N.; Dann, A.; Rodoni, B.C.; Constable, F.E. Updating the quarantine status of prunus infecting viruses in Australia. *Viruses* **2020**, *12*, 246. [[CrossRef](#)]
42. Parizipour, M.H.G.; Keshavarz-Tohid, V. Identification and phylogenetic analysis of a tobamovirus causing hibiscus (*Hibiscus rosa-sinensis* L.) mosaic disease in Iran. *J. Plant Pathol.* **2020**, *102*, 813–824. [[CrossRef](#)]
43. Kimaru, S.L.; Kilalo, D.C.; Muiru, W.M.; Kimenju, J.W.; Thuku, C.R. Molecular Detection of Cucumber Mosaic Virus and Tobacco Mosaic Virus Infecting African Nightshades (*Solanum scabrum* Miller). *Int. J. Agron.* **2020**, *2020*, 8864499. [[CrossRef](#)]
44. Afreen, B.; Baghel, G.; Fatma, M.; Usman, M.; Naqvi, Q.A. Studies on molecular detection of Cucumber mosaic virus and its anatomical and biochemical changes in *Daucus carota* L. *Int. J. Genet. Eng. Biotechnol.* **2010**, *1*, 187–192.
45. El-Attar, A.K.; Mokbel, S.A.; El-Banna, O.-H.M. Molecular Characterization of Alfalfa Mosaic Virus and Its Effect on Basil (*Ocimum basilicum*) Tissues in Egypt. *J. Virol. Sci.* **2019**, *5*, 97–113.
46. Khalil, R.R.; Bassiouny, F.M.; El-Dougoud, K.A.; Abo-Elmaty, S.; Yousef, M.S. A dramatic physiological and anatomical changes of tomato plants infecting with tomato yellow leaf curl geminivirus. *Int. J. Agric. Technol.* **2014**, *10*, 1213–1229.
47. Das, P.P.; Lin, Q.; Wong, S.M. Comparative proteomics of Tobacco mosaic virus-infected *Nicotiana tabacum* plants identified major host proteins involved in photosystems and plant defence. *J. Proteom.* **2019**, *194*, 191–199. [[CrossRef](#)] [[PubMed](#)]
48. Zhao, J.; Zhang, X.; Hong, Y.; Liu, Y. Chloroplast in Plant-Virus Interaction. *Front. Microbiol.* **2016**, *7*, 1565. [[CrossRef](#)]
49. Jamila Alfaras, A.M.; Khairiah, J.; Ismail, B.S.; Noraini, T. Effects of heavy metal exposure on the morphological and microscopical characteristics of the paddy plant. *J. Environ. Biol.* **2016**, *37*, 955–963.
50. Wahab, W.A.; Talip, N.; Basir, S.; Akbar, M.A.; Saad, M.F.M.; Bunawan, H. Disease Development and Discovery of Anatomically Resistant Features towards Bacterial Leaf Streak in Rice. *Agriculture* **2022**, *12*, 629. [[CrossRef](#)]
51. Fortes, I.M.; Fernández-muñoz, R.; Moriones, E. Host plant resistance to Bemisia tabaci to control damage caused in tomato plants by the emerging crinivirus tomato chlorosis virus. *Front. Plant Sci.* **2020**, *11*, 585510. [[CrossRef](#)] [[PubMed](#)]
52. Simon, N.M.L.; Sugisaka, J.; Honjo, M.N.; Tunstad, S.A.; Tunna, G.; Kudoh, H.; Dodd, A.N. Altered stomatal patterning accompanies a trichome dimorphism in a natural population of Arabidopsis. *Plant Direct* **2020**, *4*, e00262. [[CrossRef](#)]
53. Gonçalves, Z.S.; Lima, L.K.S.; Soares, T.L.; Abreu, E.F.M.; Barbosa, C.D.J.; Cerqueira-Silva, C.B.M.; de Jesus, O.N.; de Oliveira, E.J. de Identification of Passiflora spp. genotypes resistant to Cowpea aphid-borne mosaic virus and leaf anatomical response under controlled conditions. *Sci. Hortic.* **2018**, *231*, 166–178. [[CrossRef](#)]
54. Kappagantu, M.; Collum, T.D.; Dardick, C.; Culver, J.N. Viral Hacks of the Plant Vasculature: The Role of Phloem Alterations in Systemic Virus Infection. *Annu. Rev. Virol.* **2020**, *7*, 351–370. [[CrossRef](#)] [[PubMed](#)]
55. Talip, N.; Abdul Rahman, M.R.; Ahmad Juhari, M.A.A. *Anatomi Dan Mikroskopik Tumbuhan*; UKM Press: Bangi, Malaysia, 2019; ISBN 9789674128487.
56. Che Amri, C.N.A.B.; Mohammad Mokhtar, N.A.B.; Shahari, R. Leaf Anatomy and Micromorphology of Selected Plant Species in Coastal Area of Kuantan, Pahang, Malaysia. *Sci. Herit. J.* **2019**, *3*, 22–25. [[CrossRef](#)]
57. Mérillon, J.-M.; Ramawat, K.G. *Plant Defence: Biological Control*; Springer: Cham, Switzerland, 2020; ISBN 9783030510336.

58. Korth, K.L.; Doege, S.J.; Park, S.H.; Goggin, F.L.; Wang, Q.; Gomez, S.K.; Liu, G.; Jia, L.; Nakata, P.A. Medicago truncatula mutants demonstrate the role of plant calcium oxalate crystals as an effective defense against chewing insects. *Plant Physiol.* **2006**, *141*, 188–195. [[CrossRef](#)]
59. Tooulakou, G.; Giannopoulos, A.; Nikolopoulos, D.; Bresta, P.; Dotsika, E.; Orkoulou, M.G.; Kontoyannis, C.G.; Fasseas, C.; Liakopoulos, G.; Klapa, M.I.; et al. Alarm photosynthesis: Calcium oxalate crystals as an internal CO₂ source in plants. *Plant Physiol.* **2016**, *171*, 2577–2585. [[CrossRef](#)]
60. Karabourniotis, G.; Horner, H.T.; Bresta, P.; Nikolopoulos, D.; Liakopoulos, G. New insights into the functions of carbon–calcium inclusions in plants. *New Phytol.* **2020**, *228*, 845–854. [[CrossRef](#)] [[PubMed](#)]
61. Ziv, C.; Zhao, Z.; Gao, Y.G.; Xia, Y. Multifunctional roles of plant cuticle during plant–pathogen interactions. *Front. Plant Sci.* **2018**, *9*, 1088. [[CrossRef](#)]
62. Chwil, M.; Nurzyńska-Wierdak, R.; Chwil, S.; Matraszek, R.; Neugebauerová, J. Histochemistry and micromorphological diversity of glandular trichomes in *Melissa officinalis* L. Leaf epidermis. *Acta Sci. Pol. Hortorum Cultus* **2016**, *15*, 153–172.
63. Melotto, M.; Zhang, L.; Oblessuc, P.R.; He, S.Y. Stomatal defense a decade later. *Plant Physiol.* **2017**, *174*, 561–571. [[CrossRef](#)] [[PubMed](#)]
64. Manacorda, C.A.; Gudesblat, G.; Sutka, M.; Peluso, F.; Oricchio, P.; Baroli, I.; Asurmendi, S.; Alemano, S.; Peluso, F.; Oricchio, P.; et al. TuMV triggers stomatal closure but reduces drought tolerance in Arabidopsis. *bioRxiv* **2020**. bioRxiv:2020.08.03.235234. [[CrossRef](#)]
65. Al Basir, F.; Adhurya, S.; Banerjee, M.; Venturino, E.; Ray, S. Modelling the Effect of Incubation and Latent Periods on the Dynamics of Vector-Borne Plant Viral Diseases. *Bull. Math. Biol.* **2020**, *82*, 94. [[CrossRef](#)]
66. Funayama-Noguchi, S.; Terashima, I. Effects of Eupatorium yellow vein virus infection on photosynthetic rate, chlorophyll content and chloroplast structure in leaves of *Eupatorium makinoi* during leaf development. *Funct. Plant Biol.* **2006**, *33*, 165–175. [[CrossRef](#)]
67. Rimbaud, L.; Dallot, S.; Delaunay, A.; Borron, S.; Soubeyrand, S.; Thébaud, G.; Jacquot, E. Assessing the mismatch between incubation and latent periods for vector-borne diseases: The case of sharka. *Phytopathology* **2015**, *105*, 1408–1416. [[CrossRef](#)] [[PubMed](#)]

Disclaimer/Publisher’s Note: The statements, opinions and data contained in all publications are solely those of the individual author(s) and contributor(s) and not of MDPI and/or the editor(s). MDPI and/or the editor(s) disclaim responsibility for any injury to people or property resulting from any ideas, methods, instructions or products referred to in the content.